JJMIE

Volume 15, Number 1, March. 2021
ISSN 1995-6665
Pages 73 - 82

Jordan Journal of Mechanical and Industrial Engineering

Electromechanical Coupling Model of AC Asynchronous Motor Drive System Based on Multiscale Method

Qiuping Pan*, Jiaxiang Zhang

College of Electrical Engineering, Zhengzhou Railway Vocational & Technical College, Zhengzhou 451460, China

Received July 18 2020 *Accepted March 13 2021*

Abstract

Due to the development of motor drive system towards high power, integration and high-power density, this model cannot control mechanical vibration caused by electromechanical coupling. A new electromechanical coupling model of alternating current (AC) induction motor drive system is proposed. The transient characteristics of the motor were studied by multi-scale method, and the electromechanical coupling dynamic characteristics of the drive system were extracted. According to the dynamometer, the impact load is applied to the drive system, which causes the load on the inertial flywheel to suddenly increase by 3.5 times from 2500 Nm. The service coefficient of the realization shaft is defined as the ratio of the measured post-impact torque to the average pre-impact torque. The experimental results show that when the AC asynchronous motor's influence is passed through the electromechanical coupling model, the difference between the input and output shafts of the gearbox is minimal, and when the AC asynchronous motor's influence is different, the input and output shafts of the gearbox are maximum. It can be seen that the electromechanical coupling model established in this paper can control the mechanical vibration caused by electromechanical coupling and convert the internal load threat to the external load threat.

Keywords: multiscale method; AC asynchronous motor; drive system; electromechanical coupling model;

1. Introduction

All kinds of electromechanical systems generally have the phenomenon of electromechanical coupling. The general electromechanical systems are composed of mechanical system, electrical system and coupling magnetic field. The mechanical coupling parameters include displacement, angle, force, moment, speed and acceleration; the electromagnetic coupling parameters include voltage, current, magnetic field strength and air gap permeability. In the electromechanical system, a variety of physical processes exist at the same time, integrating all the dynamic processes. Its essence is to connect the mechanical system with the electrical system by coupling the magnetic field, so as to achieve the purpose of energy transfer [1]. It can be said that "coupling" has become an important feature of electromechanical system. On the one hand, it determines the function generation of the system, and it is the form that the system relies on to achieve its functional objectives; on the other hand, it determines the operation performance of the system. Traditional methods study different electromechanical coupling models for AC asynchronous motor, which are used to control the use of AC asynchronous motor. However, after many tests, it is found that there are some disadvantages in this model. Therefore, aiming at this question, the electromechanical coupling model of AC asynchronous motor drive system based on multiscale method is studied.

In essence, almost all scientific and engineering problems are multiscale. At the atomic scale, matter is made up of nuclei and electrons. Meanwhile, atomic time is marked in femtoseconds (10-15 seconds). In everyday life, time scales are known to be much larger. Therefore, in the face of some special problems, scales that are easily perceived are generally called macroscopic scales, while very small scales are called microscopic scales. In many cases, multi-scale effects are not that important. The equivalent physical and mathematical models of microprocesses are considered and satisfactory results are obtained. Most real-life scientific models are based on this assumption [2]. For example, in the study of fluid motion, people pay more attention to the change of fluid density and the distribution of flow field. For the molecular scale microscopic processes, the equation of state and the constitutive model are used to describe. These equivalent models are generally built on the micro scale, based on a lot of theoretical derivation and work accumulation, and have achieved many successful applications, but also have obvious limitations. The most obvious limitation is its accuracy. For complex systems, when the modeling error greatly exceeds the solving error, the practicability of the model is problematic. In addition, for those who are interested in microscopic mechanisms, the equivalent model can only be ignored blindly; Finally, for some complex systems, the equivalent models are often based on empirical formulas without strict theoretical basis. Therefore, people are more inclined to use micro scale models with higher accuracy and more complete physical and theoretical models. However, this is not the best choice,

* Corresponding author e-mail: panqiuping19881020@126.com.

and the result will be huge preprocessing effort and redundant data. Therefore, the multi-scale method came into being. Multi-scale method is one of the main research directions in the development of science and technology. It is a science that studies the modeling and solving methods of coupling phenomena between important features of different spatial and temporal scales. Through the coupling of different scale models, [3] fully absorbed the advantages of simple and efficient macroscopic scale and more accurate microscopic scale. Literature [3] proposed a model reference adaptive control (MRAC) method for the intelligent control of permanent magnet AC servo system. The system can identify parameters online and modify the network teacher values, which has strong robustness. But the accuracy of this method is low. Literature [4] proposed a design method of sliding mode fuzzy controller based on Sugeno type fuzzy reasoning and applied this method to the design of position controller of AC servo system of permanent magnet synchronous motor, which has good dynamic following performance and strong robustness, and effectively weakens the jitter. But the control of this method is not stableherefore, the basic research task of electromechanical coupling of AC induction motor drive system by using the proposed method is to study reasonable equivalent methods and coupling methods between different scales according to the required computational accuracy, as to obtain the required information more efficiently and accurately.

2. Electromechanical coupling model of AC asynchronous motor drive system based on multiscale method

2.1. Study of motor transient characteristics based on multiscale method

There are many different schemes which can be used to discretize the equations of motion and to establish the step-by-step numerical integration formula. In the field of computational science, the central difference method is widely used. It is based on the central difference formula of acceleration and velocity. The simulation time $0 \le t \le t_1$ is divided into $n=1$ to n^* steps with time interval Δt_n. n^* is the number of time steps; t_1 is the end time of the simulation; l_n is the displacement vector of the n-th time step. It is known that during the working process of the AC asynchronous motor drive system, with the deformation of the element in the calculation process, the change of the element characteristic size and the change of the critical stability integration step length will be caused. Therefore, this paper takes the explicit integration method with variable time step as an example, and Figure 1 is the schematic diagram of the time-domain discrete effect of the central difference method [4].

The time increment relationship is defined as formula (1):

$$\begin{cases} \Delta t_{n+\frac{1}{2}} = t_{n=1} - t_1 \\ t_{1+\frac{1}{2}} = \frac{1}{2}\left(t_{n=1} + t_1\right) \\ \Delta t_n = t_{1+\frac{1}{2}} - t_{1-\frac{1}{2}} \end{cases} \tag{1}$$

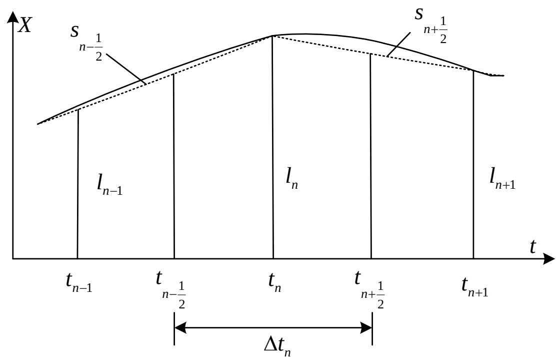

Figure 1. Time-domain discretization of central difference method

The central difference scheme of velocity is defined as follows:

$$l'_{n+\frac{1}{2}} = s_{n+\frac{1}{2}} = \frac{l_{n+1} - l_n}{t_{n+1} - t_1} = \frac{1}{\Delta t_{1+\frac{1}{2}}}\left(l_{n+1} - l_n\right) \tag{2}$$

Then the corresponding displacement recurrence formula is:

$$l_{n+1} = l_n + \Delta t_{n+\frac{1}{2}} \cdot s_{n+\frac{1}{2}} \tag{3}$$

The expression of acceleration is:

$$c_n = l''_n = \frac{1}{\Delta t_n}\left(l'_{n+\frac{1}{2}} - l'_{n-\frac{1}{2}}\right) \tag{4}$$

The corresponding speed expression is:

$$s_{n+\frac{1}{2}} = s_{n-\frac{1}{2}} + \Delta t_n \cdot c_n \tag{5}$$

In the above formula: s_n represents velocity; c_n represents acceleration. According to Figure 1 and the above derivation process, the central difference method in the multiscale method defines the speed at the midpoint of the time interval. The relationship between acceleration and displacement can be obtained by taking the above formula into formula (3):

$$c_n = l''_n = \frac{\Delta t_{n+\frac{1}{2}} \cdot \left(l_{n+1} - l_n\right) - \Delta t_{n-\frac{1}{2}} \cdot \left(l_n - l_{n-1}\right)}{\Delta t_{n+\frac{1}{2}} \cdot \Delta t_{n-\frac{1}{2}} \cdot \Delta t_n} \tag{6}$$

In the case of equal step size, the above formula is simplified as:

$$c_n = l''_n = \frac{1}{\Delta t^2}\left(l_{n+1} - 2l_n + l_{n-1}\right) \tag{7}$$

With the above discrete scheme, the integration of the motion equations in the time domain is discussed. Without considering the damping temporarily, the following formula is given in the n-th step:

$$Kc_n = \lambda_n = W_n^{(in)} - Ml_n = W_n^{(in)} - W_n^{(out)} \tag{8}$$

The above formula is a second-order ordinary differential equation for time, where $W_n^{(in)}$ and $W_n^{(out)}$ represent internal and external nodal forces, Ml_n and λ_n is a function of displacement and time [5]. The internal joint force is related to the displacement of the structure, while the external joint force is usually time-dependent but may also be related to the displacement of the joint. According to the constitutive equation of the AC asynchronous motor and the strain and strain rate of the element, the element stress is solved, and then the internal node force is obtained, while the strain and strain rate are directly determined by the displacement and its derivative. The update format of node speed is:

$$s_{n+\frac{1}{2}} = s_{n-\frac{1}{2}} + \Delta t K^{-1} \lambda_n \tag{9}$$

Given the time step n, the node force . l_n, the constitutive equation and the external force of the node, so that the $s_{n+\frac{1}{2}}$ can be solved by the above formula, and the l_{n+1} can be obtained by combining the formula (3). When the mass matrix K is simplified reasonably, it becomes a diagonal matrix, so that the updating of node velocity and displacement can be realized without solving any equation, which is conducive to saving memory and dealing with large-scale questions, which is the significant advantage and feature of the multiscale method. Using the multiscale method with central difference proposed above, the transient characteristics of the motor are studied [6].

2.2. Extraction of electromechanical coupling dynamic characteristics of drive system

The centralized parameter method is used to analyze the dynamic characteristics of the gear system. The following assumptions are adopted in the process:

1. Each gear and rotor component is simplified to a lumped mass (inertia);
2. (2) Each gear is an involute spur gear. The meshing force between gears always acts on the meshing surface and is perpendicular to the contact line of the tooth surface.
3. Gear pair, bearing and transmission shafting are simplified to be connected by concentrated stiffness and damping.
4. The friction between the teeth is ignored.
5. The mass, size and other structural parameters of the same planetary gear are the same.
6. The damping in the system is viscous damping.
7. Each gear only considers three degrees of freedom in its own plane, including translational vibration along the radial direction and torsional movement along the axial direction.
8. Assuming that the box body is a rigid body, the influence of its mass and stiffness on the drive system is ignored [7].

The translation and torsion mode of the AC asynchronous motor drive system is shown in Figure 2.

In the figure, r_i is the radius of the gear; g_{12} is the time-varying meshing stiffness of the gear pair; z_{12} is the meshing damping; b_{12} is the comprehensive meshing error; β_{12} is the meshing angle; g' is the radial support stiffness of the gear; g'' is the radial support damping of the gear; Z_i is the rotation moment of the motor drive system; α_i is the rotation angle of the gear $i\,(i=1,2)$, and its expression is:

$$\alpha_i(t) = \int \mu_i(t)\,dt + h_i(t) \tag{10}$$

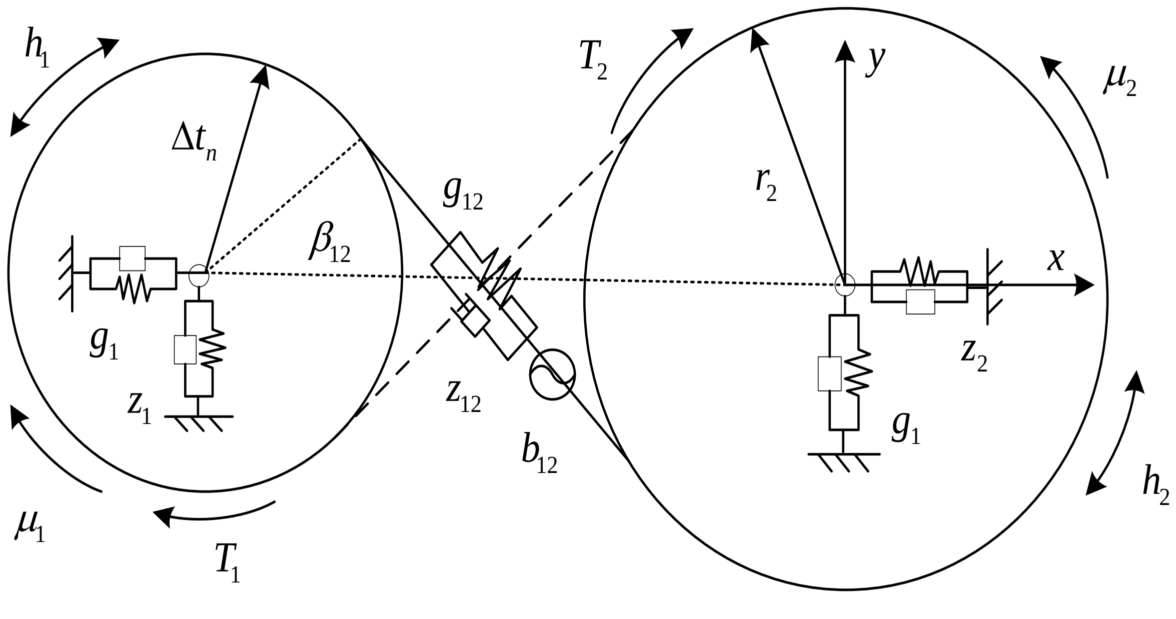

Figure 2. Translation and torsion diagram of AC asynchronous motor drive system

In the formula: μ_i is the rotational angular velocity of the rigid body of gear i, which is determined by the moment of prime mover and load in real time. This term has not been considered in the previous lumped parameter model of gear transmission; h_i is the angular displacement of elastic torsional vibration superimposed on the rigid body motion. In the past, researchers set the speed of gear as known, and reflect the law of speed change through the frequency of meshing stiffness. When running in the unsteady state, affected by the electric part of the motor and the external load of the system, the gear speed and meshing period are random and time-varying, so it is inconvenient to use time description. However, it is noted that no matter how the rotating speed changes, the active and passive gears rotate a pitch angle in each meshing cycle. Therefore, the gear angle can be used instead of time to represent the meshing cycle, that is:

$$\begin{cases} T = \dfrac{2\pi}{C_1\mu_1} \\ \alpha = \dfrac{2\pi}{C_1} \end{cases} \tag{11}$$

In the formula, T and α represent the meshing period of gear pair measured by time and angle respectively; C_1 represents the number of teeth of driving gear. Furthermore, the time-varying meshing stiffness and the comprehensive meshing error are fitted to a function that changes with the fixed period of the gear angle by the Fourier series method.

$$\begin{cases} g_{12}(\alpha_1) = \bar{g}_{12} + \sum_{d=1}^{\infty} \eta_d \cos\left[d\left(C_1\alpha_1 + \theta_{12}\right)\right] \\ b_{12}(\alpha_1, \alpha_2) = Q_{12}\sin\left(C_1\alpha_1 + \varepsilon_{12}\right) + \\ \qquad Q_1 \sin\left(\alpha_1 + \kappa_1\right) + \\ \qquad Q_2 \sin\left(\alpha_2 + \kappa_2 + \beta_{12}\right) \end{cases} \tag{12}$$

In the formula, $\bar{g}_{12}$ represents the average value of meshing stiffness in a meshing period, which can be obtained by potential energy method; η_d represents the expansion coefficient of Fourier series, $\eta_d = \dfrac{-1.5g\sin\left[d\pi\left[2-e_\beta\right]\right]}{d\pi}$, where g represents the meshing stiffness in single tooth area, e_β represents the coincidence degree; d represents the harmonic number; θ_{12} represents the initial phase of meshing stiffness; Q_{12} represents the meshing frequency error; κ_1 represents the initial phase of error respectively [8]. The time-varying of meshing damping is ignored, so the meshing damping is expressed as a linear time invariant parameter

$$z_{12} = 2\varepsilon_{12}\sqrt{\bar{g}_{12} \cdot \frac{u_1 u_2}{u_1 + u_2}} \tag{13}$$

In the formula, ε_{12} represents the meshing damping ratio, generally within the range of $0.03 \sim 0.17$; u_1 and u_2 represent the mass of adjacent gears. Considering the three meshing states of gear tooth surface contact, separation and tooth back contact, the tooth surface meshing deformation $\zeta_{12}^{q'}$ and tooth back meshing deformation $\zeta_{12}^{q''}$ of the fixed shaft gear pair can be expressed as follows:

$$\begin{cases} \zeta_{12}^{q'} = \left(x_1 - x_2\right)\sin\beta_{12} - \left(y_1 - y_2\right) \\ \zeta_{12}^{q''} = \left(x_1 - x_2\right)\sin\beta_{12} - \left(y_1 - y_2\right) \end{cases} \tag{14}$$

In the formula, x and y are the translation vibration displacements in x and y directions of gear i respectively. Accordingly, the calculation expression of meshing force F_{12} of fixed shaft gear pair is as follows:

$$\begin{gathered} F_{12} = g_{12}^{q'} f_{12}^{q'} + z_{12} f_{12}'^{q'} - g_{12}^{q''} f_{12}^{q''} - z_{12} f_{12}'^{q''} \\ g_{12}^{q'} = g_{12}(\alpha_1), g_{12}^{q''} = g_{12}\left(-\alpha_1 + \frac{1}{\pi}\right) \\ f_{12}^{q'} = \begin{cases} \zeta_{12}^{q'} & \zeta_{12}^{q'} > 0 \\ 0 & \zeta_{12}^{q'} \le 0 \end{cases}, f_{12}^{q''} = \begin{cases} \zeta_{12}^{q''} - q_{12}'' & \zeta_{12}^{q''} > q_{12}'' \\ 0 & \zeta_{12}^{q''} \le 0 \end{cases} \end{gathered} \tag{15}$$

where: $g_{12}^{q'}$ and $g_{12}^{q''}$ respectively represent the meshing stiffness when the tooth surface and the tooth back contact; $f_{12}^{q'}$ and $f_{12}^{q''}$ are used to judge the contact state of the gear pair, where q_{12}'' represents the tooth side clearance, the value of which is $q_{12}'' = \dfrac{2}{3} \times \left(0.06 + 0.0005A_{12} + 0.03K_{12}\right)$, and A_{12} is the center distance of the gear pair. Considering the rigid body rotation and elastic vibration of each gear, the translation and torsion motion equation of AC asynchronous motor is established.

$$\begin{cases} u_i\ddot{x}_i = -a_i F_{12}\sin\beta_{12} - g_i x_i - z_i\dot{x}_i \\ u_i\ddot{y}_i = a_i F_{12}\sin\beta_{12} - g_i y_i - z_i\dot{y}_i \\ G_i\ddot{\alpha}_i = a_i T_i - a_i F_{12} r_i \end{cases} \tag{16}$$

In the formula: G_i represents the moment of inertia of gear i; $a_i = 1$ corresponds to the driving gear on the left side of Fig. 2, and $a_i = -1$ corresponds to the rotating gear on the right side of Fig. 2. According to the above process, the electromechanical coupling dynamics of the drive system is analyzed and extracted [9].

2.3. Extraction of operation characteristics of AC asynchronous motor

AC asynchronous motor is a high order, nonlinear, strong coupling multivariable system. Some basic assumptions are usually made in the research:

1. It is assumed that the three-phase winding is symmetrical and the difference between them is 120 ° in space. The generated magnetomotive force is sinusoidal along the air gap;
2. Ignoring the saturation of magnetic circuit, the self-inductance and mutual inductance of each winding are constant;
3. Core loss is ignored;
4. The influence of frequency change and temperature change on winding resistance is not considered.

A control test is a functional requirement that implements a requirement definition for a single logical function and determines whether the requirement really should be reflected in the requirement.The dynamic model of AC asynchronous motor includes voltage balance equation, Newton equation, flux equation and torque equation. Among them, the number of voltage balance equations is related to the number of winding sets. N set of winding includes N differential equations [10]. The stator-side's voltage balance equation of three-phase winding motor can be written as follows:

$$U = RI + \frac{d\Psi}{dt} \tag{17}$$

wherein

$$U = [U_A, U_B, U_C, U_a, U_b, U_c] \tag{18}$$

$$I = [I_A, I_B, I_C, I_a, I_b, I_c] \tag{19}$$

$$R = \begin{bmatrix} R_s & 0 & 0 & 0 & 0 & 0 \\ 0 & R_s & 0 & 0 & 0 & 0 \\ 0 & 0 & R_s & 0 & 0 & 0 \\ 0 & 0 & 0 & R_a & 0 & 0 \\ 0 & 0 & 0 & 0 & R_b & 0 \\ 0 & 0 & 0 & 0 & 0 & R_c \end{bmatrix} \tag{20}$$

The flux equation at the stator side can be written as follows:

$$\Psi = HI \tag{21}$$

Then the inductance matrix is:

$$H = \begin{bmatrix} L_{AA} & L_{AB} & L_{AC} & L_{Aa} & L_{Ab} & L_{Ac} \\ L_{BA} & L_{BB} & L_{BC} & L_{Ba} & L_{Bb} & L_{Bc} \\ L_{CA} & L_{CB} & L_{CC} & L_{Ca} & L_{Cb} & L_{Cc} \\ L_{aA} & L_{aA} & L_{aA} & L_{aa} & L_{ab} & L_{ab} \\ L_{bA} & L_{bA} & L_{bA} & L_{ba} & L_{bb} & L_{bc} \\ L_{cA} & L_{cA} & L_{cA} & L_{ca} & L_{cb} & L_{cc} \end{bmatrix} \tag{22}$$

where, the diagonal elements in the matrix are self-inductance of each winding, and the rest are mutual inductance between corresponding windings. It is known that the stator winding of AC asynchronous motor is three-phase, the spatial difference of winding is $\frac{2}{3}\pi$, and all phases have a non-zero mutual inductance, which will cause the voltage balance equation to be very complex in the modeling process, and the model can be simplified by equivalent transformation to two-phase coordinates [11]. The stator phase current is equal to the magnetomotive force divided by the number of turns of the stator phase winding. The two-phase equivalent motor is composed of two orthogonal windings. The vector j can be considered as the sum of two independent phase current vectors projected on the $\alpha-\beta$ orthogonal coordinate system, and the mutual inductance between the two orthogonal windings is zero. When the two-phase equivalent transformation is introduced, the same flux, magnetic energy and torque should be ensured as the initial three-phase motor. This requires that the amplitude and spatial direction of the magnetomotive force O of the stator remain unchanged.

$$\begin{bmatrix} j_\alpha \\ j_\beta \end{bmatrix} = \gamma_1 \begin{bmatrix} 1 & -\frac{1}{2} & -\frac{1}{2} \\ 0 & \frac{\sqrt{3}}{2} & -\frac{\sqrt{3}}{2} \end{bmatrix} \begin{bmatrix} j_a \\ j_b \\ j_c \end{bmatrix} \tag{23}$$

$$\begin{bmatrix} u_\alpha \\ u_\beta \end{bmatrix} = \gamma_2 \begin{bmatrix} 1 & -\frac{1}{2} & -\frac{1}{2} \\ 0 & \frac{\sqrt{3}}{2} & -\frac{\sqrt{3}}{2} \end{bmatrix} \begin{bmatrix} u_a \\ u_b \\ u_c \end{bmatrix} \tag{24}$$

$$\begin{bmatrix} \tau_\alpha \\ \tau_\beta \end{bmatrix} = \gamma_3 \begin{bmatrix} 1 & -\frac{1}{2} & -\frac{1}{2} \\ 0 & \frac{\sqrt{3}}{2} & -\frac{\sqrt{3}}{2} \end{bmatrix} \begin{bmatrix} \tau_a \\ \tau_b \\ \tau_c \end{bmatrix} \tag{25}$$

In the formula, γ_1, γ_2 and γ_3 represent the adjustment coefficients of different parameters. At this time, the number of winding turns of two-phase equivalent motor needs to be increased to 1.5 times of the previous one. After conversion, the voltage and current amplitude, impedance and inductance remain unchanged, and the power $P_{\alpha\beta} = \frac{2}{3} P_{abc}$ [12]. Then the flux equation is:

$$\begin{bmatrix} \tau_{s\alpha} \\ \tau_{s\beta} \\ \tau_{r\alpha} \\ \tau_{s\beta} \end{bmatrix} = \begin{bmatrix} H_s & 0 & H_m\cos\theta_m & -H_m\sin\theta_m \\ 0 & H_s & H_m\sin\theta_m & H_m\cos\theta_m \\ H_m\cos\theta_m & H_m\sin\theta_m & H_r & 0 \\ -H_m\sin\theta_m & H_m\cos\theta_m & 0 & H_r \end{bmatrix} \begin{bmatrix} j_{s\alpha} \\ j_{s\beta} \\ j_{r\alpha} \\ j_{s\beta} \end{bmatrix} \tag{26}$$

According to the above flux equation, the operation characteristics of AC asynchronous motor are extracted. Based on this, the electromechanical coupling model of AC asynchronous motor drive system based on multiscale method is constructed.

2.4. Establishment of electromechanical coupling model considering rotor eccentricity of asynchronous motor

As the energy source of the rolling mill drive system, the dynamic behavior of the motor directly affects the performance of the main drive system of the rolling mill. For example, motor current has harmonics, motor speed and electromagnetic torque fluctuations affect the load. The motor with eccentric stator produces cogging torque with harmonic and unbalanced magnetic pull, while the rotor with eccentric rotor produces harmonic and Uniform Magnatic Field (UMF) cogging torque, and the number of poles is ± 1st harmonic. Many researchers have studied the dynamic behavior of motor. The control equations of motor rotation and electromagnetic behavior are derived. The transient dynamic characteristics of the motor with dynamic rotor eccentricity and unbalanced electromagnetic excitation are studied by using multiscale method. The unbalanced magnetic torque of the motor is analyzed by using Fourier series to determine the electromagnetic force. The electromagnetic force is introduced into the motor translation motion equation, and it is considered that the electromagnetic behavior affects the mechanical behavior, but the mechanical behavior can not affect electromagnetic behavior. However, in a real motor, there is an interaction between mechanical and electromagnetic behaviors. Therefore, it is necessary to study the dynamic behavior of the motor by deriving the control equation considering the interaction between mechanical and electromagnetic behaviors. In this study, the dynamic behavior of the motor is studied when the mechanical and electromagnetic interaction of the motor changes and the air gap between the stator and rotor changes. Considering the translational and rotational motion of the rotor, the nonlinear equation based on Lagrangian equation is derived by using dynamics and energetics, and the dynamic characteristics and mechanical and electromagnetic interaction of the motor are analyzed [13-15]. The effects of motor eccentricity on stator current, electromagnetic torque and rotor speed are studied.

Rotor eccentricity is generally divided into static eccentricity, dynamic eccentricity and mixed eccentricity. Static eccentricity means that the geometric center of the rotor is the center of rotation, and the centers of the stator and the rotor are not coincident. That is, the fixed position of the rotor in a certain direction of the stator is eccentric and rotates. At this time, no matter how the rotor rotates, the minimum position M of the rotor air gap does not change, and the air gap length does not change in the spatial distribution of the motor. This situation is generally caused by installation error or inaccurate processing of parts. Rotor dynamic eccentricity refers to that the rotor takes the stator center as the rotation center, the position of air gap in space changes with time, the minimum position of air gap changes constantly, and the length of air gap changes with the rotor rotation. Dynamic eccentricity is easy to occur in the condition of bearing damage, main shaft bending and misalignment of rotor and stator center during installation. The geometry of the motor's rotor eccentricity is shown in Figure 3 below.

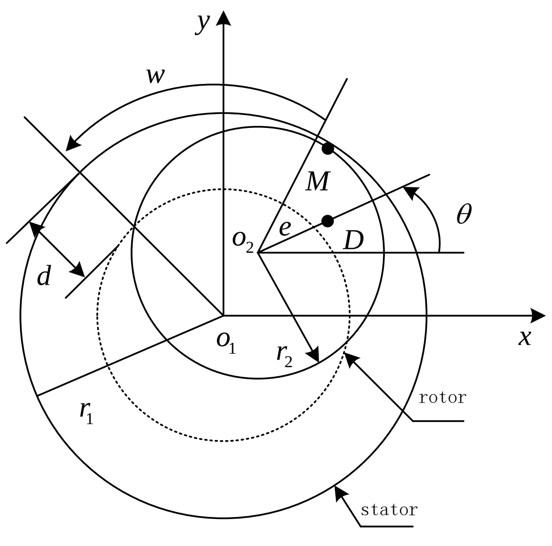

Figure 3. Geometry of rotor eccentricity

Mixed eccentricity refers to the situation that static eccentricity and dynamic eccentricity occur at the same time. Let the geometric center of the stator be o_1, the geometric center of the rotor be o_2; r_1 and r_2 are the stator radius and the rotor radius respectively. When the rotor appears eccentricity, the dotted line position of the rotor moves to the solid line position, the mass center D of the rotor rotates, and the rotation angle is expressed by θ. At this time, the air gap between the rotor and the stator at w will no longer be constant, that is, the air gap length d will change; the eccentric length between o_2 and D is expressed by e. Taking the point as the coordinate center, the $x-y$ coordinate system is established [16]. According to the coordinate system, the relative eccentricity is obtained. The kinetic energy of the drive system can be expressed as:

$$E = E_r + \frac{1}{2}\delta\theta_d^2 \tag{27}$$

In the formula, δ represents the moment of inertia of the rotor under relative eccentricity. The potential energy of the drive system is expressed as:

$$V = V_r + \frac{1}{2}\xi\left(\theta - \theta_d\right)^2 \tag{28}$$

where: ξ is the elasticity coefficient of rotor shaft. According to the Lagrange theorem, the equations are obtained.

$$\frac{d}{dt}\left[\frac{dE}{\partial\sigma}\right] + \frac{\partial F}{\partial\sigma} - \frac{\partial\left(E - V + U\right)}{\partial\sigma} = L \tag{29}$$

In the formula, σ is the generalized coordinate, which is the generalized moment of x, y and z. If $L_x = L_y = O$, $L_\theta = T_e$, then according to the above equation, the electromechanical coupling model with mechanical and electromagnetic interaction is obtained

$$\begin{cases} m\ddot{x} - me\ddot{\theta}\sin\theta - me\dot{\theta}^2\cos\theta + a_1\dot{x} + \xi x = F_x \\ m\ddot{y} - me\ddot{\theta}\cos\theta - me\dot{\theta}^2\sin\theta + a_1\dot{y} + \xi y = F_y \\ \left(\delta + me^2\right)\ddot{\theta} - me\ddot{x}\sin\theta + me\ddot{y}\cos\theta + a_2\dot{\theta} = T_e - T_s \\ T_s = \xi\left(\theta - \theta_d\right) \\ \delta_d\ddot{\theta}_d = T_s - T_d \end{cases} \tag{30}$$

In the formula: a_1 represents the equivalent damping coefficient of the rotor's translational motion; a_2 represents the equivalent damping coefficient of the rotor's rotational motion. So far, the electromechanical coupling model of AC asynchronous motor drive system based on multiscale method has been constructed [17].

3. Experimental study

In order to verify the reliability of the control effect of the electromechanical coupling model for the AC asynchronous motor drive system, the experimental platform of AC asynchronous motor drive system is built to carry out the experimental research on the dynamic characteristics of the system under the impact load condition, as more comprehensive and real dynamic characteristics of the motor gear drive system are obtained. The experimental results of the model established in this paper are compared with that of the traditional electromechanical coupling model, to provide the experimental basis for the dynamic design, condition monitoring and load shedding control of the drive system.

3.1. Experiment process

In order to maintain the similarity between the experimental system and the drive system, the main structural features of the drive system are preserved in the design of the experimental bench: between the driving motor and the drive system, a slender elastic shaft is set to simulate the AC asynchronous elastic torque shaft, and between the loading device and the drive system, an inertia flywheel is set to simulate the AC asynchronous large inertia roller. Because the motor drive system has many stages and high failure rate, in order to reduce the number of parts and improve the reliability of the system, the research plans to use the NGWN (planetary reducer) type of planetary gear transmission with large speed ratio instead of the multi-stage gear drive system of the AC asynchronous motor. Therefore, the NGWN type of planetary gear box with large speed ratio is developed and used in this experimental platform. In view of the difference between the experimental gearbox and the AC asynchronous motor drive system, when arranging the sensors, the dynamic characteristics of the area with similar structure to the drive system are mainly concerned, such as the dynamic load on the connecting shaft of the elastic shaft and the inertia flywheel and the dynamic response of the motor current. The common questions of the test-bed and the AC asynchronous motor drive system can be verified by experiments, including: the dynamic load response law of the drive system under variable speed and variable load conditions, the influence law of the torsional vibration of the drive system on the motor current, the effectiveness of the speed control strategy and the influence of different speed control strategies on the load state of the system. Figure 4 is the actual picture of the gear drive system test-bed.

The measurement and control system and software based on Disk Space Management Command (dSPACE) are designed and developed. The control system can realize the following functions: control the drive motor and the dynamometer on-line, control the start and stop of the drive motor and the dynamometer in the loading system through dSPACE, switch the speed/torque control mode and send the speed/torque target command value; monitor and collect the sensor speed, torque and current signals in real time through the QuantumX data acquisition system, and save the collected data to provide data support for the subsequent experimental analysis; the system has the ability to ensure the safe operation of the experimental platform and error command processing, to carry out safety limits on the key parameters of the system, and to have the function of emergency shutdown; the main subsystem of the measurement and control system is modularized to facilitate the subsequent improvement of the control system design. After the test platform and test system run without exception, the experiment is started.

3.2. Test and analysis

The speed of the drive motor is controlled at 600r / min by the frequency converter, and the impact load is applied to the drive system by the dynamometer, so that the load on the inertia flywheel suddenly increases by 3.5 times from 2500 Nm. The service coefficient of shaft is defined as the ratio of the measured value of torque after impact to the average value of torque before impact, and the dynamic load coefficient is the ratio of the measured value of torque during steady-state phase to the average value of torque. Taking the model constructed in this study as the test object of the experimental group, and the model constructed by two traditional methods as the test object of the control group, Figure 5 below is the comparison result of service factor of input and output shaft of gearbox at the moment of impact of AC asynchronous motor under the application of three models.

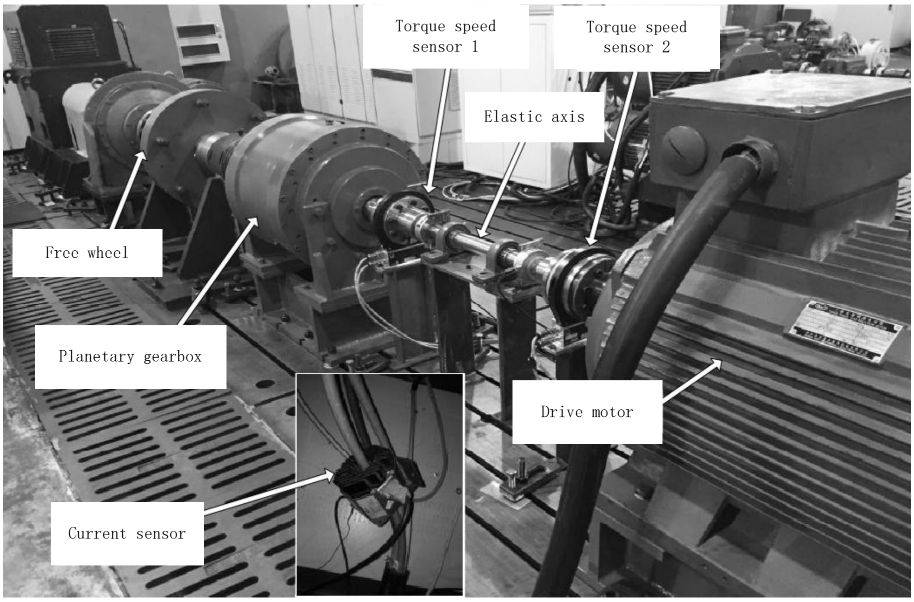

Figure 4. Actual picture of experimental platform

According to Figure 5 (a) above, there is no obvious difference between the maximum service coefficient of high-speed stage and low-speed stage in the experimental group, because the planetary transmission structure is relatively compact under the control of electromechanical coupling model. In the control group 1, the high-speed stage and low-speed stage use coefficient have a large difference, which shows that the control effect of electromechanical coupling model is poor, and the operation effect of planetary transmission structure is poor. The high-speed and low-speed use coefficients of control group 2 are also significantly different, which showed the same questions with control group 2. The experiment is carried out for two times in total, and the difference of service coefficient of high-speed stage and low-speed stage of the three test groups is shown in Table 1.

Table 1. Differences of service factor

Number of test	Experimental group	Control group 1	Control group 2
1st	0.78	0.472	0.545
2nd	0.71	0.495	0.520

According to Table 1, in the experimental group, the difference of service factor between high-speed stage and low-speed stage is very small, while the difference of service factor between the control groups is relatively large. The electromechanical coupling model in this study has better control effect on the planetary transmission structure. Under the application of the three models, Figure 6 below shows the dynamic load coefficient comparison results of the input and output shafts of the gearbox after the impact of the AC asynchronous motor.

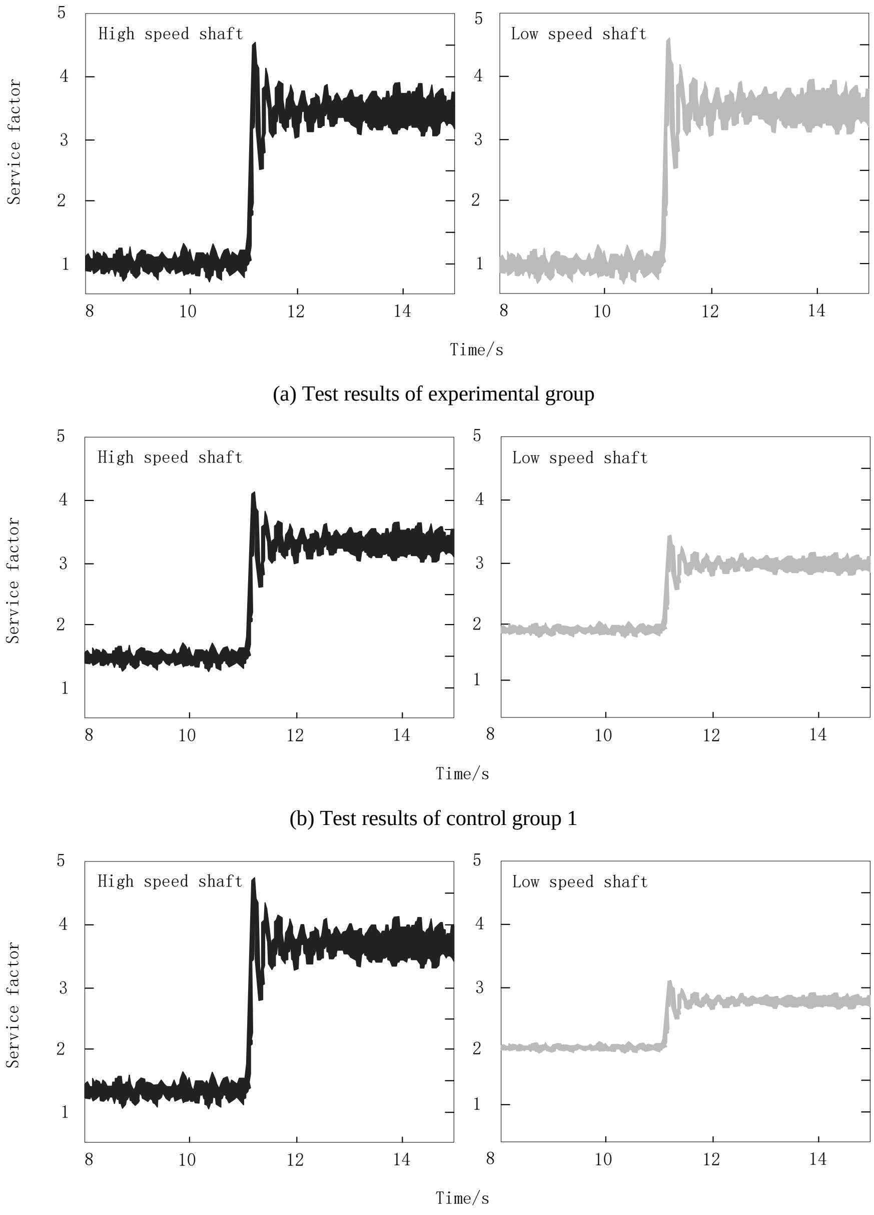

(a) Test results of experimental group

(b) Test results of control group 1

(c) Test results of control group 2

Figure 5. Test results of service factor at impact moment

According to Figure 6, the dynamic load coefficient of the experimental group decreases from the high-speed stage to the low-speed stage. After the load is increased, the service coefficient increases and the dynamic load coefficient decreases. It shows that under the control of the electromechanical coupling model, the dynamic load caused by the internal excitation such as load increase, meshing stiffness, meshing error and so on reduces the threat to the safe operation of the system, and the external load becomes the main threat. However, the dynamic load coefficient of the two control groups does not decrease due to the large difference of service coefficient, which shows that the dynamic load caused by internal excitation such as load aggravation, meshing stiffness and meshing error in the two control groups does not weaken the threat to the safe operation of the drive system, and the main threat to the motor is the internal load of the motor. In the same two tests, Table 2 below shows the test results of dynamic load coefficient in three test groups.

Table 2. Difference of dynamic load coefficient

Number of test	Experimental group	Control group 1	Control group 2
1st	0.887	0.65	0.142
2nd	0.864	0.59	0.107

According to the calculation results in Table 2, the dynamic load coefficient difference of the experimental group is the largest, while the dynamic load coefficient difference of the two control groups is very small, which shows that only the dynamic load coefficient of the experimental group is significantly reduced under the premise of increasing the service coefficient. According to the above experimental results, the electromechanical coupling model can control the normal operation of the AC asynchronous motor and the drive system, so that the AC asynchronous motor can work normally.

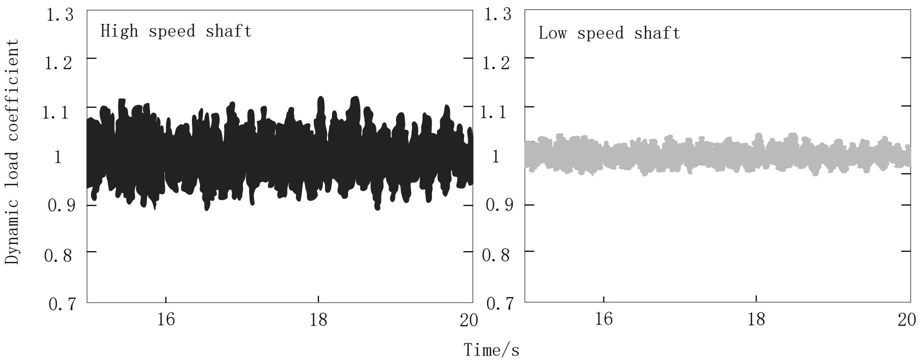

(a) Test results of experimental group

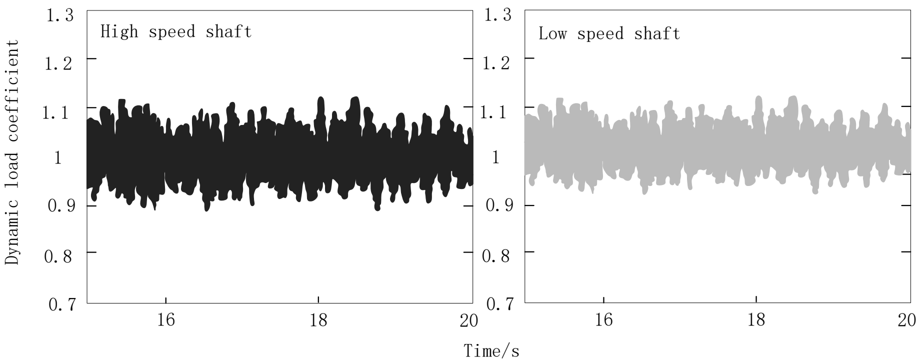

(b) Test results of control group 1

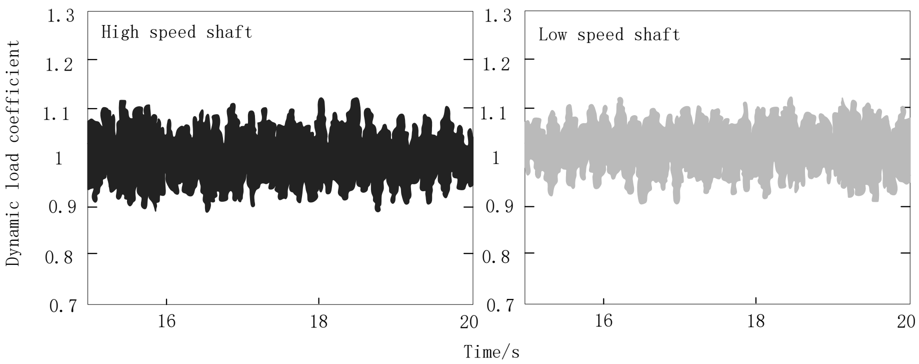

(b) Test results of control group 2

Figure 6. Dynamic load coefficient after impact

4. Conclusions

With the increase of load, the amplitude of gear meshing stiffness and bearing support stiffness increases, which leads to the increase of natural frequency in different degrees, and the increase speed slows down with the increase of load. Transient torsional vibration of the first mode is generated. In this paper, a new type of electromechanical coupling model of AC induction motor drive system is proposed. Under the control of electromechanical coupling model, the load caused by internal excitation increases. Dynamic loads such as meshing stiffness and meshing error reduce the threat to the safe operation of the system. At the moment of impact, the magnetic field of the motor can absorb part of the mechanical impact energy and play a role of buffer and protection to the driving system. It is concluded that the coupling vibration of motor gear reduces the load coefficient from high speed to low speed under stable load, and improves the internal vibration state of high speed gear safety gear train.

References

[1] Zanegin, S.; Ivanov, N.; Shishov, D.; et al. (2020) Manufacturing and testing of AC HTS-2 coil for small electrical motor. Journal of Superconductivity and Novel Magnetism, 33(2):355-359.

[2] Abboud, N.; Scovazzi, G. (2018) Elastoplasticity with linear tetrahedral elements: A variational multiscale method. International Journal for Numerical Methods in Engineering, 115(8):913-955.

[3] Vu, V.H.; Trouette, B.; TO, Q.D.; et al. (2018) Hybrid atomistic-continuum multiscale method for fluid flow with density variation in microchannels. International Journal of Numerical Methods for Heat & Fluid Flow, 28(1):3-30.

[4] Xing, Y.F.; Gao, Y.H. (2019) Multiscale eigenelement method for periodical composites: A review. Chinese Journal of Aeronautics, 32(01):104-113.

[5] Huang, Y.F.; Lu, J.F.; Ming, P.B. (2018) A concurrent global–local numerical method for multiscale PDEs. Journal of Scientific Computing, 76(2):1188-1215.

[6] Fang, Y.N.; Liang, X.H.; Zuo, M.J. (2018) Effects of friction and stochastic load on transient characteristics of a spur gear pair. Nonlinear Dynamics, 93(2):599-609.

[7] Kumar, P.; Kumar, N. Effect of EGR on performance and emission characteristics of a dual fuel engine fuelled with CNG and JOME. Biofuels, 2016.

[8] Tan, J.J.; Zhu, C.C.; Song, C.S.; et al. (2019) Effects of flexibility and suspension configuration of main shaft on dynamic characteristics of wind turbine drivetrain. Chinese Journal of Mechanical Engineering, 32(1):1-15.

[9] Fernández-Mariño, A.I.; Harpole, T.J.; Oelstrom, K.; et al. (2018) Gating interaction maps reveal a noncanonical electromechanical coupling mode in the Shaker K^+ channel. Nature Structural & Molecular Biology, 25(4):320-326.

[10] Vysotsky, V.F.; Gulyaev, I.V.; Nagirniak, A.A.; et al. (2019) Features of an asynchronous motor with a double-layer rotor in ship pumping equipment. Russian Electrical Engineering, 90(1):1-5.

[11] Zheng, J.C.; Wang, Y.; Lin, C.C.; et al. (2018) A fusion algorithm of target dynamic information for asynchronous multi-sensors. Microsystem Technologies, 24(10):3995-4005.

[12] Chuang, H.C.; Li, G.D.; Lee, C.T. (2019) The efficiency improvement of AC induction motor with constant frequency technology. Energy, 174:805-813.

[13] Li, J.; Sheng, P.; Shao, K. (2020) Optimization of clutchless AMT shift control strategy for electric vehicles. Jordan Journal of Mechanical and Industrial Engineering, 14(1):109-117.

[14] Zhang, Q.; Wang, Y.; Lin, W.; et al. (2020) Contact mechanics analysis and optimization of shape modification of electric vehicle gearbox. Jordan Journal of Mechanical and Industrial Engineering, 14(1):15-24.

[15] Vavilov, V.E. (2018) Influence of rotor eccentricity in ultrahigh-speed electrical machines on their characteristics. Russian Engineering Research, 38(8):617-622.

[16] Othmani, C.; Zhang, H.; Lü, C.F.; et al. (2019) Effects of initial stresses on the electromechanical coupling coefficient of SH wave propagation in multilayered PZT-5H structures. The European Physical Journal Plus, 134(11):1-18.

[17] Chu, L.L.; Li, Y.B.; Dui, G.S. (2019) Size-dependent electromechanical coupling in functionally graded flexoelectric nanocylinders. Acta Mechanica, 230(9):3071-3086.